JPE 19-2-17

https://doi.org/10.6113/JPE.2019.19.2.519
ISSN(Print): 1598-2092 / ISSN(Online): 2093-4718

Precise Modeling and Adaptive Feed-Forward Decoupling of Unified Power Quality Conditioners

Yingpin Wang†, Rubangakene Thomas Obwoya*, Zhibo Li*, Gongjie Li*, Yi Qu**, Zeyu Shi***, Feng Zhang***, and Yunxiang Xie***

†,*College of Physics and Electronic Engineering, Hainan Normal University, Hainan, China
**Hainan Province Key Laboratory of Laser Technology and photoelectric Functional Materials, Haikou, China
***School of Electric Power, South China University of Technology, Guangzhou, China

Abstract

The unified power quality conditioner (UPQC) is an effective custom power device that is used at the point of common coupling to protect loads from voltage and current-related PQ issues. Currently, most researchers have studied series unit and parallel unit models and an idealized transformer model. However, the interactions of the series and parallel converters in AC-link are difficult to analyze. This study utilizes an equivalent transformer model to accomplish an electric connection of series and parallel converters in the AC-link and to establishes a precise unified mathematical model of the UPQC. The strong coupling interactions of series and parallel units are analyzed, and they show a remarkable dependence on the excitation impedance of transformers. Afterward, a feed-forward decoupling method based on a unified model that contains the uncertainty components of the load impedance is applied. Thus, this study presents an adaptive method to estimate load impedance. Furthermore, simulation and experimental results verify the accuracy of the proposed modeling and decoupling algorithm.

Key words: Adaptive feed-forward decoupling, Interaction analysis, Power quality, Precise unified modeling, UPQC

I. INTRODUCTION

Recently, power quality (PQ) issues have attracted a lot of attention. PQ issues can be broadly classified into voltage problems and current problems [1]. These problems include voltage sags that decrease the efficiency of power system networks, and current harmonics that increases energy losses and reduce the life span of connected equipment. Common solutions to these problems include dynamic voltage restorers [2], active power filters [3] and unified PQ conditioners (UPQCs) [4].

Studies define UPQC as an effective custom power device that is used at the point of common coupling to protect a load from PQ issues. UPQCs can solve voltage sags, harmonics, a low power factor and three-phase unbalance. Moreover, the UPQC is a combined series and parallel converter (also called a shunt converter) used to enhance the voltage and current qualities [5].

Most researchers have focused on the control algorithms of UPQCs [6], [7] and rarely investigated their modeling. A number of studies have been conducted on the modeling of the parallel and series converters and idealized transformer models [8], [9]. Raphael J. Millnitz dos Santos considered the leakage inductance of transformers and modeled each of the converters separately [10]. A. Senthilkumarand proposed a unified equivalent circuit for UPQCs and used a series converter as the voltage source and a parallel converter as the current source [11]. Kian Hoong Kwan [12], [13] applied an L filter and an idealized transformer model to establish a unified equivalent circuit of UPQCs. However, they did not reveal the natural characteristics of UPQCs. None of the above-mentioned studies considered the effects of excitation impedance and they did not extensively analyze the interactions of the series and parallel units in the AC-link. Thus, a precise model should be established to analyze the natural characteristics of UPQCs.

Most of the decoupling studies have investigated the interaction of the d-axis and the q-axis in one converter [14], [16]. R. Modesto stated that UPQCs have strong coupling and

Manuscript received Apr. 12, 2017; accepted Nov. 17, 2018
Recommended for publication by Associate Editor Jinjun Liu.
†Corresponding Author: wangyingppp@126.com
Tel: +8615217630408, Hainan Normal University
*College of Physics & Electronic Eng., Hainan Normal Univ., China
**School of Electric Power, South China Univ. of Technol., China

decoupling from the *dq* coordinate to the *αβ* coordinate in single converters [14]. Najafi M. proposed a decoupled system consisting of separate UPQCs and wind turbines in a DC-link [15]. Ryszard S. presented a diagram with a combination of series and parallel converters decoupled in a single converter and analyzed the interactions in the DC-link [16]. Li Peng revealed that the interactions of the series and parallel units occur in the AC and DC-links. He also analyzed the interactions in the steady state and idealized conditions, and superficially eliminated the interactions. However, the natural characteristics of the coupling were not explored [17].

The coupling of the series and parallel units in the AC-link severely affects the compensation performance. Thus, the interference of the series and parallel units should be accurately decoupled to improve the compensation performance.

This study utilized an equivalent transformer model to accomplish the electric connection of the series and parallel converters in the AC-link and established a precise unified mathematical model of UPQCs. The interactions of the series and parallel units were then analyzed. Afterward, an adaptive feed-forward decoupling method based on a unified model was applied to eliminate the interference of the series and parallel units. An adaptive method was used to estimate the load impedance. Furthermore, simulations and experiments were conducted to verify the accuracy of the proposed modeling and decoupling algorithm.

II. Unified Mathematical Modeling of UPQC

At present, the most common topologies of UPQCs are grid side series and load-side parallel. Their schematics are shown in Fig. 1.

The series converter is mainly used to compensate for the voltage offset, and the parallel converter is applied to inhibit the harmonics and reactive compensation. Series and parallel converters share a DC capacitor, and this is called coupling. However, the interaction is small [15], and the interaction in the DC-link is not observed in this study.

A circuit diagram is shown in Fig. 2. The parallel converter applies an *LCL* filter and the series converter applies an *LC* filter since the transformer is equivalent to the inductance, and the filter is equivalent to the *LCL* filter. One phase is considered, where the transformation ratio is 1:1 and the three phases are symmetrical.

As shown in Fig. 2, the transformer output voltage is:

$$u_2 = \frac{z_m z_L u_1 + (z_1 z_2 + z_m(z_1+z_2))u_s - z_L(z_1 z_2 + z_m(z_1+z_2))i_p}{z_1(z_2+z_L) + z_m(z_1+z_2+z_L)}, \quad (1)$$

The transformer input voltage is:

$$u_1 = \frac{z_c}{z_c+z_f}u_i - \frac{z_f z_c}{z_c+z_f}i_1, \quad (2)$$

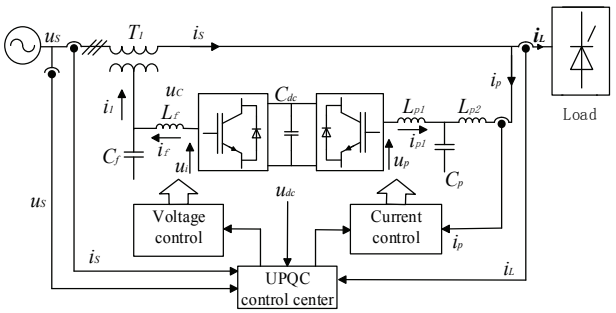

Fig. 1. Schematic of a grid side series and load side parallel UPQC.

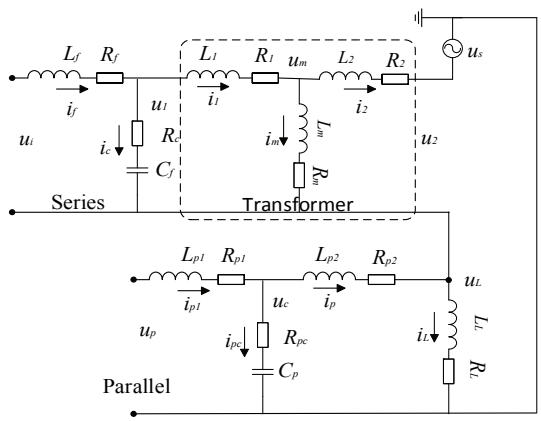

Fig. 2. Circuit diagram of a UPQC in one phase.

The transformer input current is:

$$i_1 = \frac{z_L+z_2+z_m+z_s}{z_m(z_L+z_s)}u_2 - \frac{z_2+z_m}{z_m(z_L+z_s)}u_s + \frac{z_L(z_2+z_m)}{z_m(z_L+z_s)}i_p, \quad (3)$$

The parallel injecting current is:

$$i_p = \frac{z_{pc}u_p - (z_{p1}+z_{pc})(u_s-u_2)}{z_{p2}z_{p1} + z_{pc}(z_{p1}+z_{p2})}, \quad (4)$$

where $z_f = R_f + L_f s$, $z_c = R_c + \frac{1}{C_f s}$, $z_1 = R_1 + L_1 s$, $z_m = R_m + L_m s$, $z_2 = R_2 + L_2 s$, $z_L = R_L + L_L s$, $z_{p1} = R_{p1} + L_{p1} s$, $z_{pc} = R_{pc} + \frac{1}{C_p s}$, and $z_{p2} = R_{p2} + L_{p2} s$.

In an idealized transformer model, the transformer output voltage u_2 is equal the input voltage u_1, and the output current i_2 is equal to the input current i_1. In other words, the leakage inductances z_1 and z_2 are equal to zero, and the excitation impedance z_m is infinite. Consequently, the impact of the transformer leakage inductance and excitation impedance are negligible. In fact, an equivalent transformer model can precisely indicate the transformer, as shown in Fig. 2. In the MATLAB simulation, the excitation impedance z_m was calculated by the transformer capacitor P_N and rating voltage V_N, as shown in Equ. (5), and the leakage inductances z_1 and z_2 were set to 1% of excitation impedance. In the experiment, the transformer parameters were obtained from no-load and short-

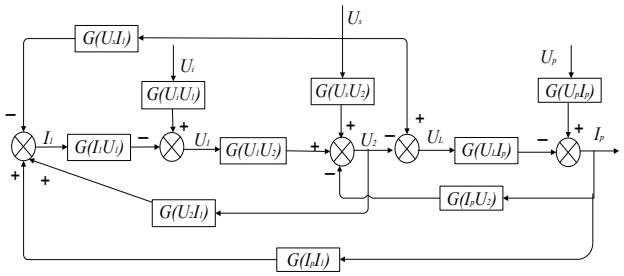

Fig. 3. Transfer relationship of a UPQC.

circuit tests. The following modeling and simulation indicate that the transformer leakage inductance and excitation are important in terms of device performance. Thus, these factors should be modeled in an equivalent transformer model.

$$R_m=\omega L_m=\frac{V_N^2}{P_N}, \tag{5}$$

where ω is the angular frequency (commonly equal to 100π).

III. Interaction Analysis of Series and Parallel Units

As shown in Fig. 2, the state equations were difficult to establish considering that the unified circuit of a UPQC was an improper network. Thus, a transfer relationship was established based on equations (1)-(4), as shown in Fig. 3. where:

$$G(U_2I_1)=\frac{z_L+z_2+z_m}{z_mz_L}, \tag{6}$$

$$G(U_sI_1)=\frac{z_2+z_m}{z_mz_L}, \tag{7}$$

$$G(I_pI_1)=\frac{z_2+z_m}{z_m}, \tag{8}$$

$$G(U_1U_2)=\frac{z_mz_L}{z_1(z_2+z_L)+z_m(z_1+z_2+z_L)}, \tag{9}$$

$$G(U_sU_2)=\frac{z_1z_2+z_m(z_1+z_2)}{z_1(z_2+z_L)+z_m(z_1+z_2+z_L)}, \tag{10}$$

$$G(I_pU_2)=\frac{z_L(z_1z_2+z_m(z_1+z_2))}{z_1(z_2+z_L)+z_m(z_1+z_2+z_L)}, \tag{11}$$

$$G(U_iU_1)=\frac{z_c}{z_c+z_f}, \tag{12}$$

$$G(I_1U_1)=\frac{z_cz_f}{z_c+z_f}, \tag{13}$$

$$G(U_pI_p)=\frac{z_{pc}}{z_{p2}z_{p1}+z_{pc}(z_{p1}+z_{p2})}, \tag{14}$$

$$G(U_LI_p)=\frac{z_{pc}+z_{p1}}{z_{p2}z_{p1}+z_{pc}(z_{p1}+z_{p2})}. \tag{15}$$

A. Series Converter Output Voltage to Transformer Output Voltage

As shown in Fig. 3, the influences of the source voltage U_s and the parallel converter output voltage U_p were negligible, and the transfer function between the series converter output voltage U_i and the transformer output voltage U_2 was obtained by Equ. (16).

B. Series Converter Output Voltage to Parallel Injecting Current

As shown in Fig. 3, the influences of the source voltage U_s and the parallel converter output voltage U_p were negligible, and the transfer function between the series converter output voltage U_i and the parallel injecting current I_p was obtained by Equ. (17).

C. Parallel Converter Output Voltage to Parallel Injecting Current

As shown in Fig. 3, the influences of the source voltage U_s and the series converter output voltage U_i were negligible, and the transfer function between the parallel converter output voltage U_p and the parallel injecting current I_p was obtained by Equ. (18).

D. Parallel Converter Output Voltage to Transformer Output Voltage

As shown in Fig. 3, the influences of the source voltage U_s and the series converter output voltage U_i were negligible, and the transfer function between the parallel converter output voltage U_p and the transformer output voltage U_2 was obtained by Equ. (19).

E. Relative Gain Calculation

A UPQC control system can be considered to be a two-input and two-output system. The control system is expressed in the following transfer function matrix as:

$$\begin{bmatrix}U_2\\I_P\end{bmatrix}=\begin{bmatrix}G(U_i2U_2) & G(U_p2U_2)\\G(U_i2I_p) & G(U_p2I_p)\end{bmatrix}\begin{bmatrix}U_i\\U_p\end{bmatrix}. \tag{20}$$

A relative gain array (RGA) method is applied, where the relative gain λ_{ij} for the input u_j and the output y_i is defined by the ratio of the uncontrolled and controlled gains [18]. The RGA matrix is defined as:

$$\Lambda(\boldsymbol{G}(s))=\boldsymbol{G}(s)\times\left[\boldsymbol{G}(s)^{-1}\right]^{\mathrm{T}}, \tag{21}$$

where $\boldsymbol{G}(s)=|g_{ij}(s)|$ is the transfer function matrix in Equ. (20).

For a 2×2 system:

$$\Lambda(\boldsymbol{G}(s))=\begin{bmatrix}\lambda_{11} & \lambda_{12}\\ \lambda_{21} & \lambda_{22}\end{bmatrix}=\begin{bmatrix}\dfrac{1}{1-\gamma(s)} & \dfrac{\gamma(s)}{\gamma(s)-1}\\ \dfrac{\gamma(s)}{\gamma(s)-1} & \dfrac{1}{1-\gamma(s)}\end{bmatrix}, \tag{22}$$

where:

$$\gamma(s)=\frac{g_{12}(s)g_{21}(s)}{g_{11}(s)g_{22}(s)}. \tag{23}$$

The main relative gains are the elements of the RGA matrix in the input–output pairing. Generally, an RGA matrix is applied to analyze the degree of coupling in multi-input multi-output systems [19]. For the UPQC control system, the input signal U_i is designed to control U_2, and U_p is designed to control I_p. Thus, the main relative gains are λ_{11} and λ_{22}.

$$\lambda_{22}=\lambda_{11}=\frac{G(U_i2U_2)G(U_p2I_p)}{G(U_i2U_2)G(U_p2I_p)-G(U_p2U_2)G(U_i2I_p)} \tag{24}$$

(16), (17), (18) and (19) are substituted into (24) to obtain (25).

F. Interaction Analysis in a Bode Diagram

The system parameters are listed in Table I. As shown above, Eqns. (6)-(15) are substituted into Eqns. (16)-(19) and (25) to obtain the transfer functions, and Bode diagrams are shown in Fig. 4. The main relative gains of 20 kVA and 2000 kVA of λ_{11} in the transformer capacitor P_N are depicted as the lines "r11-P20" and "r11-P2000," respectively.

As shown in Fig. 4, the parallel output voltage U_p and the series converter output voltage U_i affect the transformer output voltage U_2 and the parallel injecting current I_p. In the UPQC control system, the series converter output voltage U_i is designed to control the transformer output voltage U_2 in a compensating voltage problem ($G(U_i2U_2)$). However, the series converter output voltage U_i affects the parallel injecting current I_p($G(U_i2I_p)\neq0$) and disturbs the compensation of the parallel converter. Similarly, the parallel converter output voltage U_p is designed to control the parallel injecting current I_p when compensating for the current problem ($G(U_p2I_p)$). This affects the transformer output voltage U_2($G(U_p2U_2)\neq0$).

TABLE I
SYSTEM PARAMETERS

Parameters	Value
RMS source voltage (U_s)	380 V
Fundamental frequency (f)	50 Hz
Series L filter (L_f/R_f)	1 mH/0.01 Ω
Series C filter (C_f/R_c)	30 μF/2 Ω
Parallel L filters (L_{p1}/R_{p1}) and (L_{p2}/R_{p2})	0.2 mH/0.02 Ω
Parallel C filter (C_p/R_{pc})	10 μF/2 Ω
Transformer capacity (P_N)	20 kVA
Transformer rated voltage (V_N)	110 V
DC-link desired voltage (V_{dc})	700 V
DC-link capacitor (C_{dc})	5000 μF

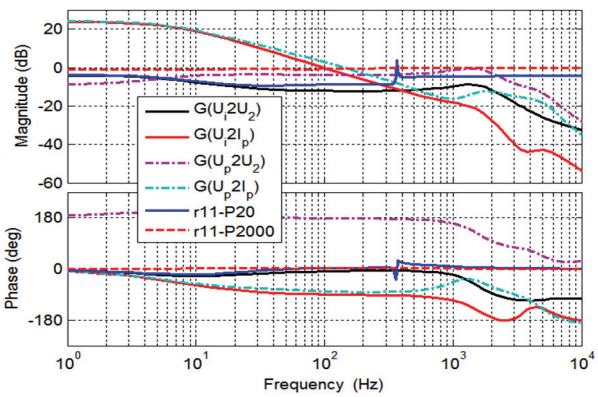

Fig. 4. Bode diagram of the UPQC interaction relationship.

The line "r11-P20" indicates that the main relative gain is low, especially at medium frequencies (10–300 Hz), which indicates that the system is strongly coupled [19]. However, in the line "r11-P2000," the main relative gain is close to 1, which indicates that the system is weakly coupled and decoupling is not required. However, the capacitor in a 2000 kVA transformer is large and expensive. The above analysis shows that the coupling relationship of the series and parallel units is highly dependent on the transformer capacitor (excitation impedance). Thus, a precise model should be established for the equivalent transformer model.

$$G(U_i2U_2)=\frac{G(U_iU_1)G(U_1U_2)}{1+G(U_LI_p)G(I_pU_2)+G(U_1U_2)G(I_1U_1)(G(U_2I_1)+G(U_LI_p)G(I_pI_1))}, \tag{16}$$

$$G(U_i2I_p)=\frac{G(U_iU_1)G(U_1U_2)G(U_LI_p)}{1+G(U_LI_p)G(I_pU_2)+G(U_1U_2)G(I_1U_1)(G(U_2I_1)+G(U_LI_p)G(I_pI_1))}, \tag{17}$$

$$G(U_p2I_p)=\frac{G(U_pI_p)(G(U_1U_2)G(I_1U_1)G(U_2I_1)+1)}{1+G(U_LI_p)G(I_pU_2)+G(U_1U_2)G(I_1U_1)(G(U_2I_1)+G(U_LI_p)G(I_pI_1))}, \tag{18}$$

$$G(U_p2U_2)=-\frac{G(U_pI_p)(G(I_pI_1)G(I_1U_1)G(U_1U_2)+G(I_pU_2))}{1+G(U_LI_p)G(I_pU_2)+G(U_1U_2)G(I_1U_1)(G(U_2I_1)+G(U_LI_p)G(I_pI_1))}, \tag{19}$$

$$\lambda_{22}=\lambda_{11}=\frac{1+G(U_1U_2)G(I_1U_1)G(U_2I_1)}{1+G(U_1U_2)G(I_1U_1)G(U_2I_1)-G(U_LI_p)(G(I_pI_1)G(I_1U_1)G(U_1U_2)+G(I_pU_2))}. \tag{25}$$

IV. Decoupling Control Algorithm

On the basis of the above analysis, the series and parallel converters are strongly coupled, and they affect the transformer output voltage and the parallel injecting current. Thus, the mutual interference should be mitigated.

A. Feed-Forward Decoupling Method

The feed-forward decoupling method is a simple and effective method. Thus, a feed-forward decoupling method based on a mathematical model can be used to mitigate the interaction of series and parallel converters. A diagram of the feed-forward decoupling method is shown in Fig. 5, where:

$$G(DU_p2U_i)=\frac{G(U_p2U_2)}{G(U_i2U_2)}=-\frac{G(U_pI_p)(G(I_pI_1)G(I_1U_1)G(U_1U_2)+G(I_pU_2))}{G(U_iU_1)G(U_1U_2)}, \quad (26)$$

$$G(DU_i2U_p)=\frac{G(U_i2I_p)}{G(U_p2I_p)}=\frac{G(U_iU_1)G(U_1U_2)G(U_LI_p)}{G(U_pI_p)(G(U_1U_2)G(I_1U_1)G(U_2I_1)+1)}, \quad (27)$$

Substituting Eqns. (6), (8), (9) and (11)-(15) into (26) and (27) yields:

$$G(DU_p2U_i)=-\frac{z_{pc}((z_2+z_m)z_cz_f+(z_c+z_f)(z_1z_2+z_m(z_1+z_2)))}{z_cz_m(z_{p1}z_{p2}+z_{pc}(z_{p1}+z_{p2}))}, \quad (28)$$

$$G(DU_i2U_p)=\frac{z_cz_mz_L(z_{p1}+z_{pc})}{z_{pc}((z_L+z_2+z_m)z_cz_f+(z_c+z_f)(z_1(z_2+z_L)+z_m(z_1+z_2+z_L)))}, \quad (29)$$

The control system without decoupling is expressed as:

The close loop of U_2 without decoupling is expressed as:

$$G(UDU_2{}_2U_2)=\frac{PI_1(G(U_i2U_2)-\frac{PI_2G(U_i2I_p)G(U_p2U_2)}{1+PI_2G(U_p2I_p)})}{1+PI_1(G(U_i2U_2)-\frac{PI_2G(U_i2I_p)G(U_p2U_2)}{1+PI_2G(U_p2I_p)})}. \quad (30)$$

The control system of series and parallel converters after decoupling are separated is expressed as:

The close loop of U_2 after decoupling is expressed as:

$$G(DU_2{}_2U_2)=\frac{PI_1G(U_i2U_2)}{1+PI_1G(U_i2U_2)}. \quad (31)$$

Bode diagrams of close loops without decoupling and after decoupling are shown in Fig. 8.

As shown in Fig. 8, the control system after decoupling is stable, whereas the control system without decoupling is unstable, and the resonance is approximately 1.5 kHz.

B. Adaptive Feed-Forward Decoupling Algorithm

As shown in Eqns. (28) and (29), the feed-forward transfer function $G(DU_p2U_i)$ is only related to the parameters of a UPQC. However, the transfer function $G(DU_i2U_p)$ contains load impedance z_L. In fact, the load impedance is uncertain, and a feed-forward method cannot completely or accurately decouple the load impedance. This study presents an adaptive feed-forward decoupling algorithm to estimate the load impedance. A nonlinear load is equivalent to a linear load and a harmonics current source. The harmonics current source is used as a disturbance, and the equivalent linear load is only considered in modeling. The equivalent linear load impedance is expressed as:

$$\vec{z}_L=Z_L(\cos\varphi+j\sin\varphi), \quad (32)$$

where Z_L is the amplitude of the load impedance, and φ is the

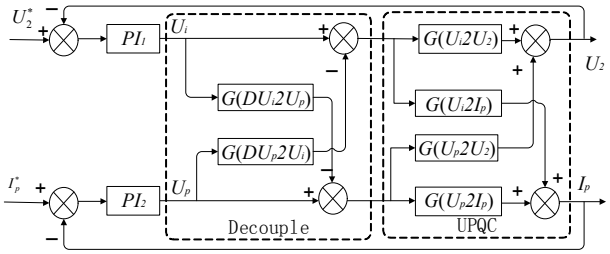

Fig. 5. Feed-forward decoupling control method of a UPQC.

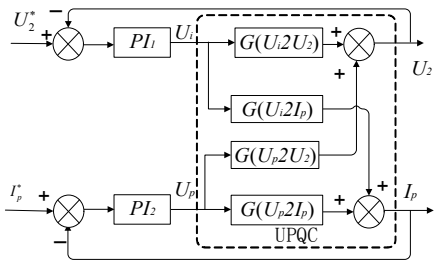

Fig. 6. Control system of voltage without decoupling.

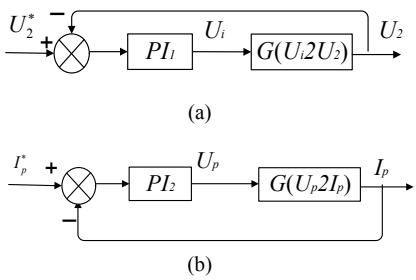

Fig. 7. Control system after decoupling. (a) Voltage control system. (b) Current control system.

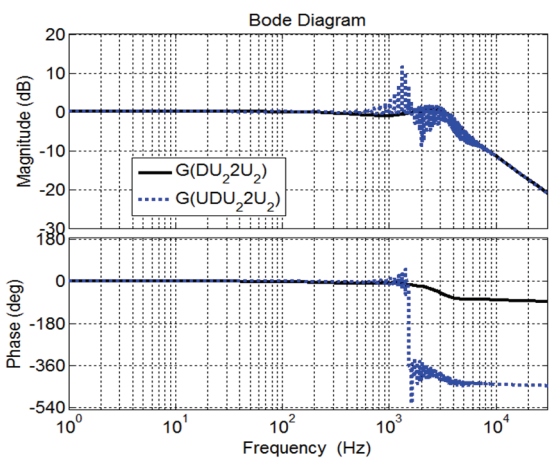

Fig. 8. Bode diagrams of decoupled and coupled controls.

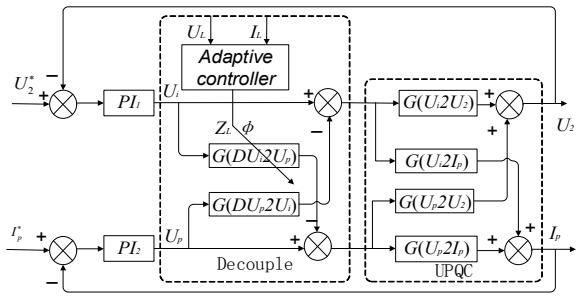

Fig. 9. Adaptive feed-forward decoupling control method of a UPQC.

angle of the impedance, which can be expressed as:

$$\vec{i}_L = \vec{u}_L / \vec{z}_L \tag{33}$$

For the *abc* reference frame, the voltage and current are periodic variations, and are transformed into the *dq* reference frame to calculate the value of the impedance [20]. Afterward, the amplitudes of the voltage U_L and the current I_L are applied to calculate the amplitude of the impedance Z_L, and impedance angle φ is calculated from i_d and i_q. Considering that the current contains harmonics, a moving average filter method is applied to obtain the DC component and to eliminate harmonics [21], as depicted in Equ. (36).

$$\hat{Z}_L = \frac{\overline{U_L}}{\overline{I_L}}, \tag{34}$$

$$\hat{\phi} = \tan^{-1}\frac{\overline{i_q}}{\overline{i_d}}, \tag{35}$$

$$\overline{x(t)} = \frac{1}{T_\omega}\int_{t-T_\omega}^{t} x(\tau)d\tau, \tag{36}$$

where T_ω = 0.01 s presents the window width, and $x(t)$ can be U_L, I_L, i_d and i_q.

On the basis of the moving average filter, the calculation can converge to an accurate value of the impedance Z_L and the impedance angle φ within 0.01 s when the load impedance changes. The adaptive decoupling algorithm is shown in Fig. 9.

V. Simulation Analysis

Simulations were conducted in MATLAB/Simulink and the simulation parameters are listed in Table I. The applied system PI control method and the parameters are PI_1 (K_{p1} = 1, K_{i1} = 500) and PI_2 (K_{p1} = 4, K_{i1} = 200). The load consisted of linear and nonlinear types, and the rated voltage was 380 V (L-L). The system was analyzed under different operating conditions as follows.

A. Case 1: Source Voltage Distortion

The compensation performance without decoupling control was compared with adaptive feed-forward decoupling control. The working condition was a source voltage with 20% of the 5th harmonic, and the load was a resistance parallel to a diode rectifier. The results of series and parallel converters without decoupling control are shown in Fig. 10. The results of series and parallel converters with adaptive feed-forward decoupling control are shown in Fig. 11.

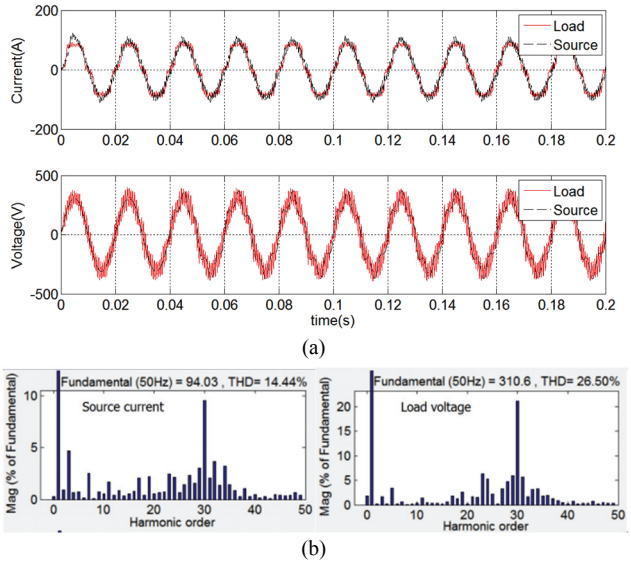

(a)

(b)

Fig. 10. Results of source voltage distortion without decoupling. (a) Results of the current and voltage. (b) THD of the source current and load voltage.

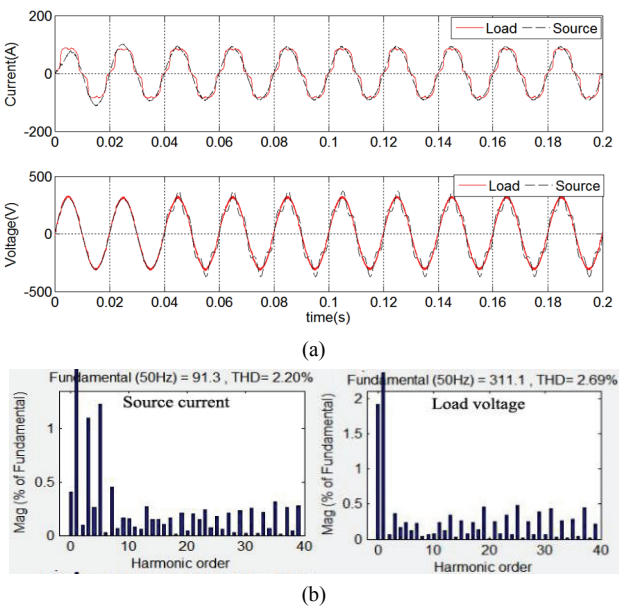

(a)

(b)

Fig. 11. Results of source voltage distortion with the proposed control. (a) Results of the current and voltage. (b) THD of the source current and load voltage.

As shown in Fig. 10, the total harmonic distortions (THDs) of the source current and load voltage are 14.44% and 26.50% when the source current and load voltage contain a lot of harmonics for approximately 30 s. This condition is due to the mutual interference of the series and parallel units, as shown in Fig. 8. As shown in Fig. 11, the THD of the source current

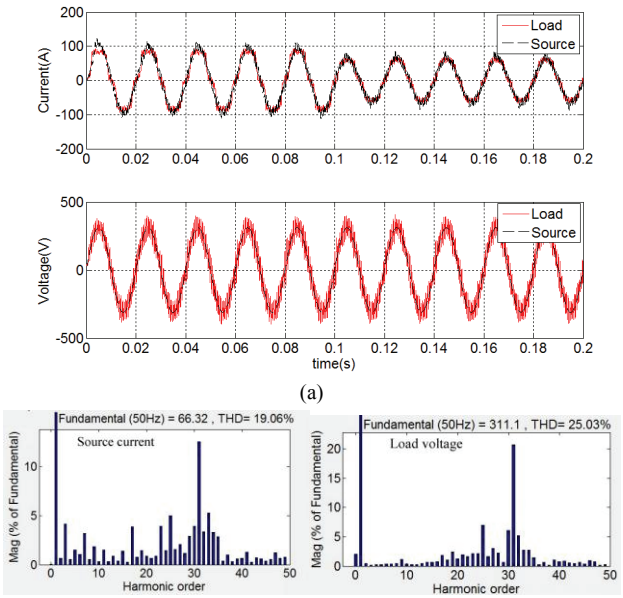

Fig. 12. Results of a load change without decoupling. (a) Results of the current and voltage. (b) THD of the source current and load voltage.

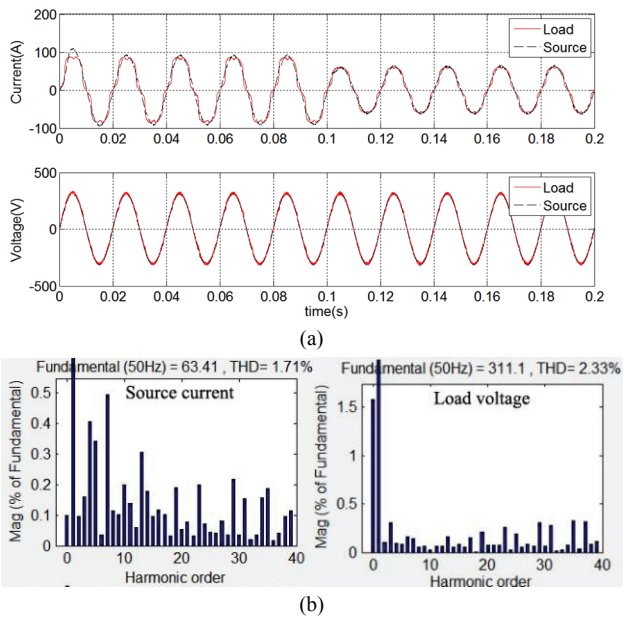

Fig. 13. Results of a load change with the proposed control. (a) Results of the current and voltage. (b) THD of the source current and load voltage.

is 2.20%, and the THD of the load voltage is 2.69% with adaptive feed-forward decoupling control, which meet the IEEE 519 standard. The above comparisons show that the adaptive feed-forward decoupling method is excellent and that the mathematical model is accurate.

B. Case 2: Load Change

The compensation performance without decoupling control is compared with adaptive feed-forward decoupling control under a load change of 0.1 s. The simulation results in the load change condition without decoupling control are shown in Fig. 12. The results of the load change condition with adaptive feed-forward decoupling control are shown in Fig. 13.

As shown in Fig. 12, the source current and load voltage without decoupling control contain large harmonics for approximately 30 s. The THD of the source current and load voltage are 19.06% and 25.03%. As shown in Fig. 13, the current compensation response is fast, and the load voltage is stable when adaptive feed-forward decoupling control is applied. The THD of load current is 18.11%. After compensation, the THD of the source current and load voltage are 1.71% and 2.33%. These results verify that the proposed algorithm performs under load changes.

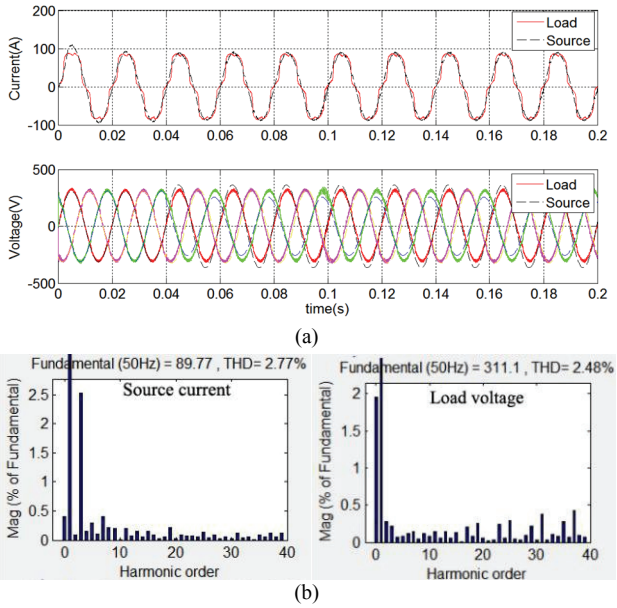

Fig. 14. Results of source voltage unbalance. (a) Results of the current and voltage. (b) THD of the source current and load voltage.

C. Case 3: Source Voltage Unbalance

Simulation results of the source voltage unbalance condition using the proposed method are shown in Fig. 14.

As shown in Fig. 14, the load current has a serious distortion, the THD is 18.32%, and the source voltage peak values are 363.8, 322.5 and 256.1 V. After compensation, the THD of the source current and load voltages are 2.77% and 2.48%, and the load voltages are 311.1, 310.8 and 310.7 V. These results demonstrate that the proposed algorithm performs well in source voltage unbalance conditions.

VI. Experimental Analysis

Experiments were implemented in a three-phase four wire UPQC prototype to validate the simulation results of the proposed algorithm. The parameters and control methods used in the experiment are the same as those used in the simulation.

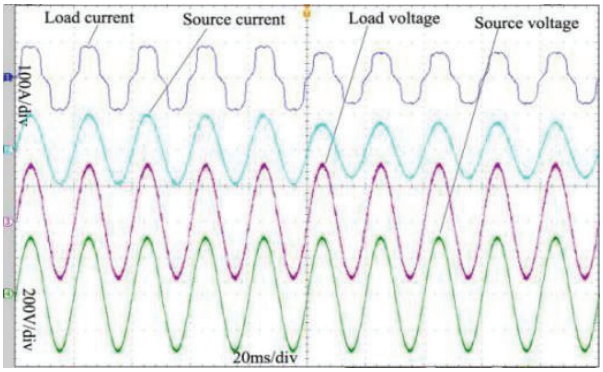

(a)

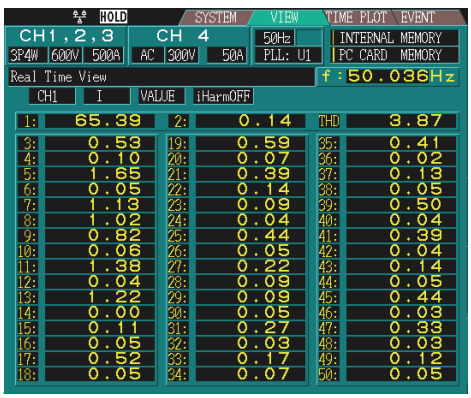

(b)

Fig. 15. Experimental results of a load change. (a) Graphs of the current and voltage. (b) THD of the source current.

Experimental waveforms are obtained by using a Tektronix oscilloscope, and the DSP is a TMS320F28335. The system is unstable without decoupling control. Thus, experiments are only conducted with the decoupling control, and are expressed under the following conditions.

A. Case 1: Load Change

Experimental results of the adaptive feed-forward decoupling algorithm under the load change condition are shown in Fig. 15.

As can be seen in Fig. 15, the UPQC achieves good current compensation and a rapid responses, and the load voltage is stable under a load change. The THD of the source current is 3.87%. Thus, the proposed algorithm performs well under load changes.

B. Case 2: Source Voltage Unbalance

Experimental results of the source voltage unbalance condition using the proposed method are shown in Fig. 16.

As shown in Fig. 16, the THD of the load current is 17.73%, and the source voltages are unbalanced. After compensation, the THD of source current is 4.57%, and load voltages are balanced.

The above simulation and experimental results verify that the mathematical model is accurate, and that the proposed algorithm is effective in compensating both voltage and current problems.

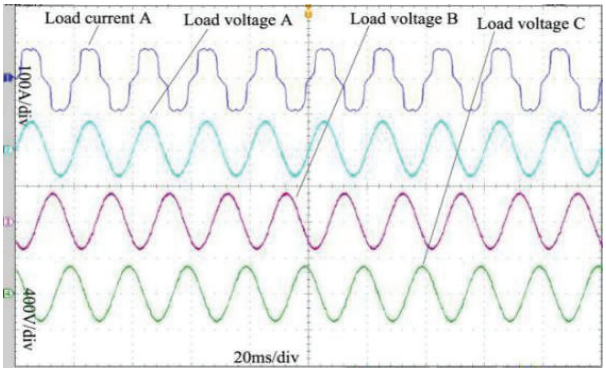

(a)

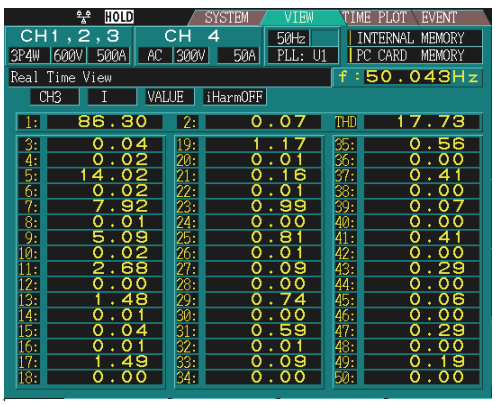

(b)

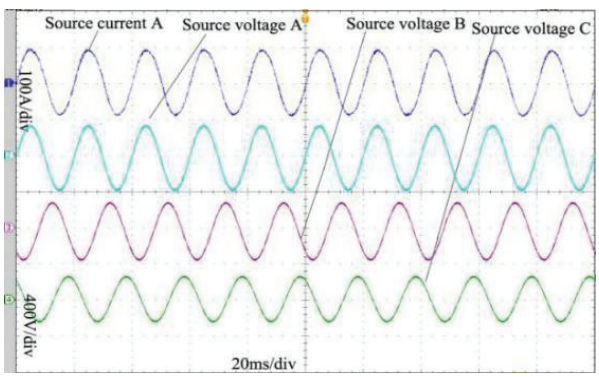

(c)

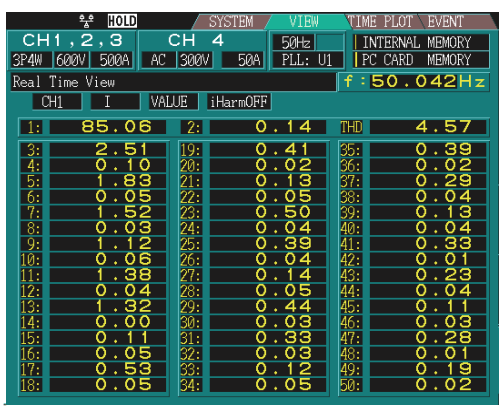

(d)

Fig. 16. Experimental results of unbalance source voltage. (a) Graphs in the load side. (b) THD of the load current. (c) Graphs in the source side. (d) THD of the source current.

VII. CONCLUSION

This study presented a precise unified mathematical model that is valuable in terms of parameter optimization, interaction analysis and control algorithm design. On the basis of the interaction analysis, the series converter and parallel converters are strongly coupled, and are mainly dependent on the excitation impedance of the transformer. The application of an adaptive feed-forward decoupling control algorithm based on the established model completely eliminated the interactions and improved the voltage and current compensation performance. Simulation and experimental results verified that the precise model is accurate and that the proposed adaptive feed-forward decoupling control algorithm remarkably improves the compensation performance.

ACKNOWLEDGMENT

This work is supported by the project of 'Natural Science Foundation of Hainan Province (No.2018CXTD336)' and 'National Natural Science Foundation of China (61864002)'.

REFERENCES

[1] B. W. Franca, L. F. Silva, M. A. Aredes, and M. Aredes, "An improved iUPQC controller to provide additional grid-voltage regulation as a STATCOM," *IEEE Trans. Ind. Electron.*, Vol. 62, No. 3, pp. 1345-1352, Mar. 2015.

[2] F. Jiang, C. Tu, Z. Shuai, M. Cheng, Z. Lan, and F. Xiao, "Multilevel cascaded-type dynamic voltage restorer with fault current-limiting function," *IEEE Trans. Power Del.*, Vol. 31, No. 3, pp. 1261-1269, Jun. 2016.

[3] P. Kanjiya, V. Khadkikar, and H. H. Zeineldin, "Optimal control of shunt active power filter to meet IEEE Std. 519 current harmonic constraints under nonideal supply condition," *IEEE Trans. Ind. Electron.*, Vol. 62, No. 2, pp. 724-734, Jul. 2015.

[4] V. Khadkikar, "Enhancing electric power quality using UPQC: A comprehensive overview," *IEEE Trans. Power Electron.*, Vol. 27, No. 5, pp. 2284-2297, May 2012.

[5] A. K. Panda and N. Patnaik, "Management of reactive power sharing & power quality improvement with SRF-PAC based UPQC under unbalanced source voltage condition," *Int. J. Electr. Power & Energy Syst.*, Vol. 84, pp. 182-194, Jan. 2017.

[6] C. Salim and B. M. Toufik, "Simplified control scheme of unified power quality conditioner based on three-phase three-level (NPC) inverter to mitigate current source harmonics and compensate all voltage disturbances," *J. Electr. Eng. Technol.*, Vol. 8, No. 3, pp. 544-558, May 2013.

[7] N. Patnaik and A. K. Panda, "Performance analysis of a 3 phase 4 wire UPQC system based on PAC based SRF controller with real time digital simulation," *Int. J. Electr. Power Energy Syst.*, Vol. 74, pp. 212-221, Jan. 2016.

[8] J. A. Munoz, J. R. Espinoza, C. R. Baier, L. A. Morán, E. E. Espinosa, P. E. Melín, and D. G. Sbárbaro, "Design of a discrete-time linear control strategy for a multicell UPQC," *IEEE Trans. Ind. Electron.*, Vol. 59, No. 10, pp. 3797-3807, Oct. 2012.

[9] R. K. Patjoshi, V. R. Kolluru, K. Mahapatra, "Power quality enhancement using fuzzy sliding mode based pulse width modulation control strategy for unified power quality conditioner," *Int. J. Electr. Power Energy Syst.*, Vol. 84, pp. 153-167, Jan. 2017.

[10] D. S. Millnitz, J. C. Cunha, and M. Mezaroba, "A simplified control technique for a dual unified power quality conditioner," *IEEE Trans. Ind. Electron.*, Vol. 61, No. 11, pp. 5851-5860, Mar. 2014.

[11] A. Senthilkumarand and P. A. Raj, "ANFIS and MRAS-PI controllers based adaptive-UPQC for power quality enhancement application," *Electr. Power Syst. Res.*, Vol. 126, pp. 1-11, Sep. 2015.

[12] K. H. Kwan, P. L. So, and Y. C. Chu, "An output regulation-based unified power quality conditioner with Kalman filters," *IEEE Trans. Ind. Electron.*, Vol. 59, No. 11, pp. 4248-4262, Apr. 2012.

[13] K. H. Kwan, Y. C. Chu, and P. L. So, "'Model-based H ∞ control of a unified power quality conditioner," *IEEE Trans. Ind. Electron.*, Vol. 56, No. 7, pp. 2493-2506, Apr. 2009.

[14] R. Modesto, S. A. O. Silva, A. A. O. Júnior, and V. D. Bacon, "Versatile unified power quality conditioner applied to a three-phase four-wire distribution systems using a dual control strategy," *IEEE Trans. Power Electron.*, Vol. 31, No. 8, pp. 5503-5516, Oct. 2016.

[15] M. Najafi, M. Siahi, R. Ebrahimi, and M. Hoseynpoor, "Economic analysis and comparison of decoupled and coupled operation of UPQC with wind energy generation system," *Australian J. Basic Applied Sci.*, Vol. 5, No. 5, pp. 417-423, Mar. 2011.

[16] S. Ryszard, B. Grzegorz, R. Jacek, and D. Henryk, "Modeling and experimental investigation of the small UPQC systems," *IEEE Compat. Power Electron.*, pp. 223-237, 2005.

[17] P. Li, Y. Li, and Z. Yin, "Realization of UPQC H∞ coordinated control in Microgrid," *Int. J. Electr. Power Energy Syst.*, Vol. 65, pp. 443-452, Feb. 2015.

[18] M. Mokhtari, J. Khazaie, D. Nazarpour, and F. Morteza, "Interaction analysis of multifunction FACTS and D-FACTS controllers by MRGA," *Turkish J. Electr. Eng. Comput. Sci.*, Vol. 21, pp. 1685-1702. Oct. 2013,

[19] D. Chen and D. E. Seborg, "Relative gain array analysis for uncertain process models," *Aiche Journal*, Vol. 2, No. 48, pp. 302-310, Feb. 2002.

[20] A. Farmann, W. Waag, and D. U. Sauer, "Adaptive approach for on-board impedance parameters and voltage estimation of lithium-ion batteries in electric vehicles," *J. Power Sources*, Vol. 299, pp. 176-188, Dec. 2015.

[21] J. Wang, J. Liang, F. Gao, L. Zhang, and Z. Wang, "A method to improve the dynamic performance of moving average filter-based PLL," *IEEE Trans. Power Electron.*, Vol. 30, No. 10, pp. 5978-5990, Dec. 2015.

Yingpin Wang was born in Hainan, China, in 1985. He received his B.S. degree in Mechanical Engineering and Automation from Jilin University, Changchun, China, in 2008. He received his M.S. degree in Mechanical Manufacturing and Automation and his Ph.D. degree in Power Electronics from the South China University of Technology, Guangzhou, China, in 2011 and 2017, respectively. From 2011 to 2012, he worked as a Mechanical Engineering at Sany Heavy Industry, Changsha, China. From 2012 to 2014, he worked as an Assistant Research Fellow at the Guangzhou Institute of Advanced Technology, Chinese Academy of Sciences, Guangzhou, China. He is presently working at Hainan Normal University, Haikou, China. His current research interests include active power filters, rectifiers and switching power supplies.

Rubagaknene Thomas Obwoya was born in Masindi, Uganda, in 1997. He is presently working towards his B.S. degree in Mechanical and Electrical Integrated Engineering, Hainan Normal University, Haikou, China. His current research interests include electrical systems and control technologies.

Zhibo Li was born in Chongqing, China, in 1982. He received his B.S. degree in Mechanical Engineering and Automation from the Nanjing Agricultural University, Nanjing, China; and his M.S. degree in Vehicle Engineering from Shandong University, Jinan, China. He is presently working as a Lecturer at Hainan Normal University, Haikou, China. His current research interests include automation, electric machine drives, and vibration and noise control.

Gongjie Li was born in Hainan, China, in 1986. He received his B.S. and M.S. degrees in Control Science and Engineering from the Harbin Institute of Technology, Harbin, China, in 2010 and 2013, respectively. He is presently working as an Assistant at Hainan Normal University, Haikou, China. His current research interests include industrial automation, motors and control.

Yi Qu was born in 1969. He received his B.S. and M.S. degrees from the Changchun Institute of Optics and Fine Mechanics, Changchun, China, in 1991 and 1999, respectively. He received his Ph.D. degree from Jilin University, Changchun, China, in 2002. From 2003 to 2005, he was a Postdoctoral Research Fellow in the School of Materials Engineering, Nanyang Technological University, Singapore. From January 2006 to October 2006, he was a Singapore Millennium Scholarships Postdoctoral Research Fellow. From February 2012 to August 2012, he was a Senior Visiting Fellow in the Department of Electrical Engineering, Yale University, New Haven, CT, USA. From 2003 to 2017, he was with the National Key Laboratory on High Power Semiconductor Lasers, Changchun University of Science and Technology, Changchun, China. Since April 2017, he has been a Professor and a Vice Director Professor of the College of Physics and Electronics Engineering, Hainan Normal University, Haikou, China. He has published over 150 papers in journals and conference proceedings. His current research interests include the fabrication and application of optoelectronics devices.

Zeyu Shi was born in Ganzhou, China, in 1991. He received his B.S. degree in Electrical Engineering from the Hefei University of Technology, Hefei, China, in 2013. He is presently working towards his Ph.D. degree in Electrical Engineering at the South China University of Technology, Guangzhou, China. His current research interests include high-power density rectifiers and control strategies.

Feng Zhang was born in Shanxi, China, 1986. He received his B.S. degree in Electrical Engineering from Lushan College, Guangxi University of Technology, Liuzhou, China, in 2010; and his M.S. degree in Control Engineering from Guangxi University, Nanning, China, in 2014. Since 2016, he has been working towards his Ph.D. degree in Power Electronics at the South China University of Technology, Guangzhou, China. His current research interests include micro-inverters and multi-level inverters for photovoltaic applications.

Yunxiang Xie received his Ph.D. degree in Electrical Engineering from Xi'an Jiaotong University, Xi'an, China, in 1991. Since 1991, he has been a Professor in the School of Electric Power, South China University of Technology, Guangzhou, China. He was a Professor at the University of Queensland, Brisbane, Australia. From 1996 to 1997, he was a Visiting Professor at the University of Western Ontario, London, ON, Canada. He is the author or coauthor of about 50 scientific papers published in international journals and conference proceeding. His research interests include power inverters, power quality, active filters, switched-mode power supplies, electric drives and digital control systems. His current research interests include power electronic converters, matrix converters, active and hybrid filters, the application of power electronics in renewable energy systems and electrified railway systems, reactive power control, harmonics, and power quality compensation systems such as SVC, UPQC and FACTS devices. Dr. Xie is a senior member of China Electro-Technical Society, and China Power Electronics Society.